

Kinetics Modeling of a Convergent Cascade Catalyzed by Monooxygenase–Alcohol Dehydrogenase Coupled Enzymes

Jennifer Engel, Uwe T. Bornscheuer, and Selin Kara*



Cite This: <https://dx.doi.org/10.1021/acs.oprd.0c00372>



Read Online

ACCESS |



Metrics & More



Article Recommendations



Supporting Information

ABSTRACT: A convergent cascade reaction coupling a cyclohexanone monooxygenase variant and an alcohol dehydrogenase to make ϵ -caprolactone from cyclohexanone and 1,6-hexanediol was characterized via progress curve analysis with two kinetic models developed iteratively. A chemical side reaction occurring with the utilized Tris buffer and consequent byproduct formations were considered in Model 2, which reduced the root-mean-square error (RMSE) values by half, compared to Model 1 (RMSE values of 13%–40%). The optimized model, Model 2, led us to simulate the cascade reaction including 22 kinetic parameters with a maximum RMSE value in the range of 10%–21%.

KEYWORDS: enzyme kinetics modeling, redox reactions, enzymatic cascade, monooxygenase, alcohol dehydrogenase

INTRODUCTION

Modeling of Enzymatic Reactions. In order to get the most efficient enzymatic reaction, in a cascade system or with a single enzyme, optimization of the reaction parameters (e.g., temperature, pH, and substrate concentration) is necessary. This can be achieved by investigating these parameters in an experimental way, either via single run experiments or “Design of Experiments” (DoE). Another option is developing a kinetic model describing the enzymatic reaction. The purely experimental way would require a vast amount of experiments, while the computational way can avoid tedious laboratory work and save resources. Nevertheless, a fewer number of experiments is still required, since developing an enzyme kinetic model requires detailed knowledge about the enzyme kinetic parameters.^{1–3} An overview of an exemplary way for enzyme kinetic modeling is shown in Figure 1.

Since the enzyme kinetic parameters are dependent on running conditions (e.g., pH, buffer and temperature, medium components, etc.), initially the reaction conditions, with respect to those have to be selected. Choosing the reaction conditions, especially in a multienzymatic system, often is a compromise between the highest activity and the stability of the enzymes under these conditions.^{3,5} Afterward, the kinetic parameters can be estimated from the experimental data. Generally, there are two different approaches for the determination of kinetic parameters: (i) initial rates measurements and (ii) progress curve analysis.^{1–3} The initial rates approach is the most common and vastly used method. It is easy to execute in the laboratory and the computational capacity is relatively low.² However, it lacks the ability to capture reaction equilibria, enzyme deactivation, decomposition of substrates and/or products, and, thus, long-term effects of the reaction.^{1,2} Furthermore, capturing product inhibition requires many experiments and, given that, might not even be described accurately.¹ Therefore, the initial rates approach can be time-, material-, and cost-intensive. In contrast, following the concentrations of reaction

components over time (namely, progress curve analysis) can compensate the limitations that the initial rate analyses has. The progress curve analysis is able to describe important long-term effects of the reaction, such as enzyme deactivation and product inhibition.² Different inhibition types do exist, which should be considered in the progress curve analysis.⁶ Nevertheless, progress curve analysis also has its bottlenecks. Over the course of time, unknown side reactions may occur that can be difficult to identify and characterize. In addition, there could be inaccuracies in the initial concentrations and reaction starting times. These challenges can also be encountered in an applied process and, therefore, must be handled. Fortunately, these issues can be solved by computational methods.² Instead of choosing between these two approaches, the initial rates approach can be used to determine starting values for the parameters, which are then refined and completed with progressive curve analysis.⁴ While the kinetic laws are formulated as reaction rates, the experimental data from the progress curve analysis are captured as concentrations. In order to derive a kinetic model, two methods can be applied: (i) the integration of the kinetic law or (ii) formulation of ordinary differential equations (ODEs) of the concentrations.^{2,3} The integration of the kinetic law can be very complex already for simple equations and, thus, are not applicable for more-complex systems. Consequently, the common way is the formulation of ODEs to describe the concentrations in relation to the kinetic laws.² The kinetic representation of an enzymatic cascade is shown to be exemplary on a linear cascade reaction with

Special Issue: Celebrating Women in Process Chemistry

Received: August 17, 2020

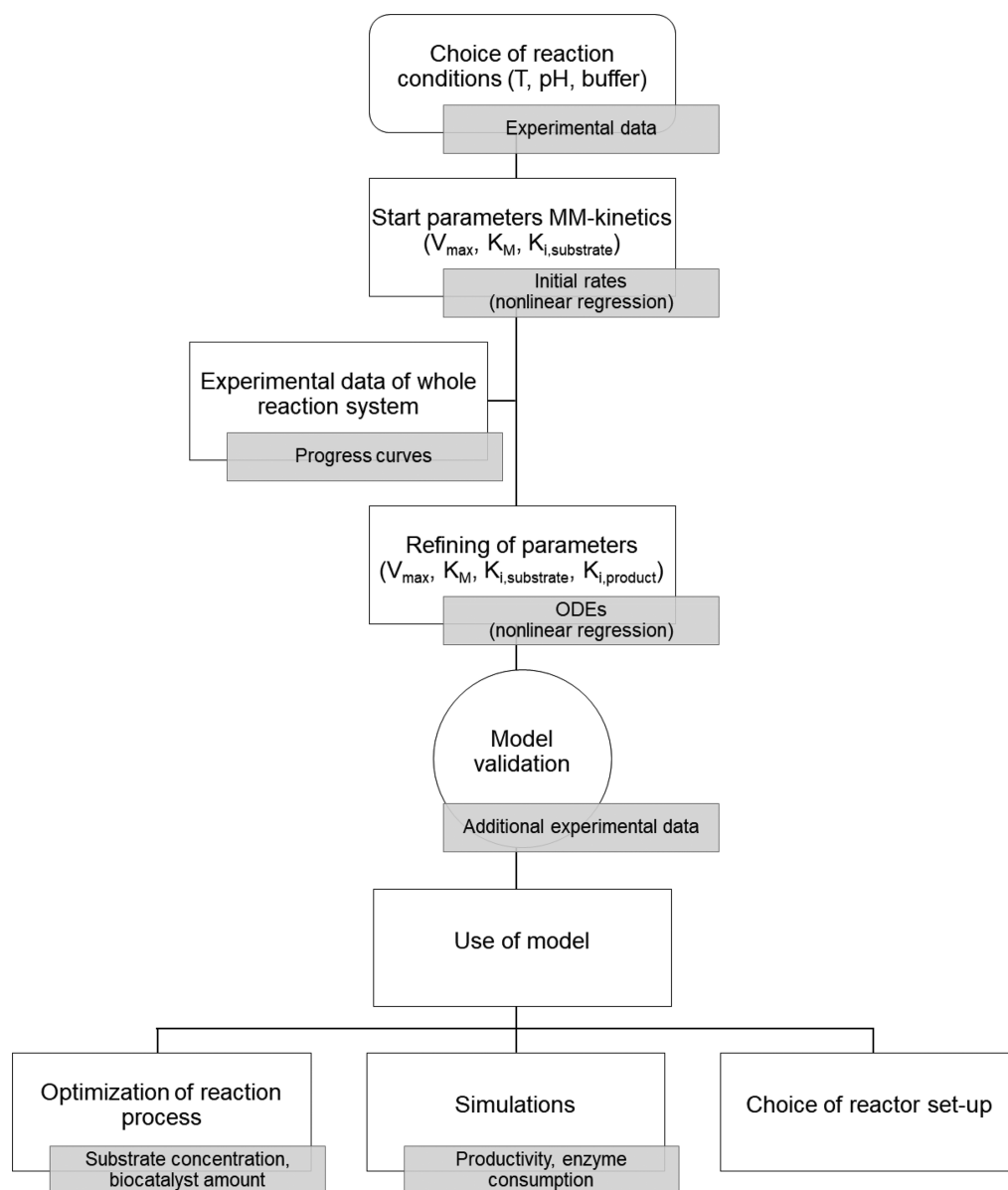
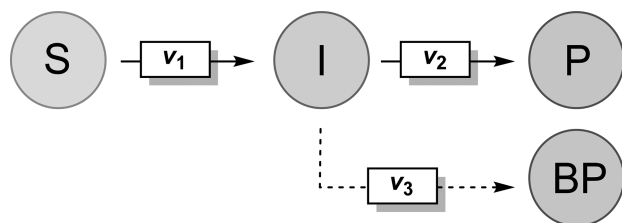


Figure 1. Flow scheme for the kinetic modeling of an enzymatic reaction. [Adapted from Vasic-Racki et al.³ and Al-Haque et al.⁴]

byproduct formation, assuming that all reaction steps are irreversible (Scheme 1, eqs 1 and 2).

Whether the individual steps in the reaction are catalyzed by the same enzyme or by several enzymes is determined using the general Michaelis–Menten equation and ODEs are not relevant. However, the concentration of the respective enzyme must be

Scheme 1. General Scheme of a Linear Enzymatic Cascade^a



^aLegend: S, substrate, I, intermediate, P, product, BP, byproduct, and v , reaction rate.

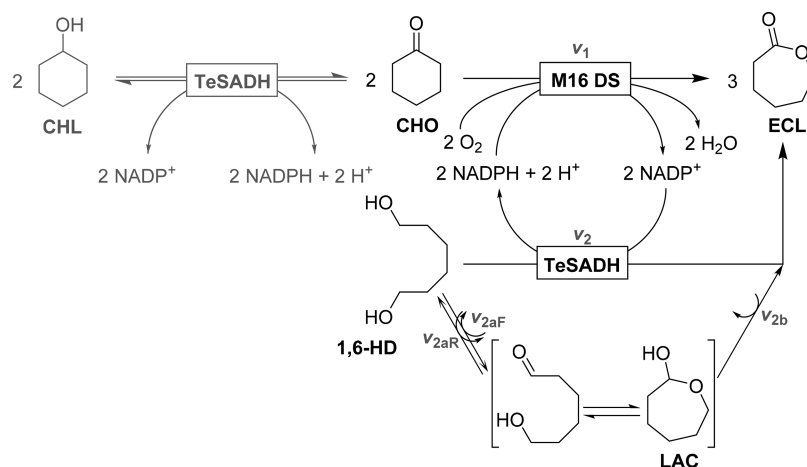
multiplied by the corresponding reaction velocity/rate. Hence, which enzyme is the catalyst (e.g., the side reaction) must be known. In addition, factors such as evaporation/hydrolysis of a substrate/product and enzyme deactivation must be considered. The enzyme deactivation can be written as a separate ODE, when deactivation is considered as a decrease in the “active” enzyme concentration.

Equation 1 gives the general Michaelis–Menten equation:

$$v_m = \frac{v_{\max,m} \times c_n}{K_{M,n} + c_n} \quad (1)$$

where m represents the reaction number ($m = 1-3$), n is the respective substrate of reactions 1–3, v denotes the reaction rate [U/mg], c is the concentration [mM], v_{\max} represents the maximum reaction rate [U/mg], and K_M is the Michaelis–Menten constant [mM].

Equation 2 defines the ODEs for the change of concentrations over the course of the reaction:

Scheme 2. Reaction Scheme of the Convergent Cascade with Assigned Rates: Model 1^a

^aLegend: CHO, cyclohexanone, 1,6-HD, 1,6-hexanediol, ECL, ϵ -caprolactone, LAC, lactol intermediate, CHL, cyclohexanol (not considered in model development).

$$f(t) = \frac{dc_s}{dt} = (-v_1 \times c_{E,1}) - x$$

$$f(t) = \frac{dc_1}{dt} = (+v_1 \times c_{E,1}) - (v_2 \times c_{E,2}) - (v_3 \times c_{E,3}) - y$$

$$f(t) = \frac{dc_p}{dt} = (+v_2 \times c_{E,2}) - z$$

$$f(t) = \frac{dc_{BP}}{dt} = +v_3 \times c_{E,3} \quad (2)$$

Here, x , y , and z are additional factors influencing the concentrations (e.g., evaporation, hydrolysis, degradation, enzyme deactivation) [mM/min]; and $c_{E,m}$ represents the concentration of the enzyme catalyzing reaction m [mg/mL].

Once the parameters are estimated and refined, the model must be validated. Therefore, simulations and experiments are conducted under the same reaction conditions.^{3,4} The numerical solution of the model is then compared with the experimentally determined concentrations.^{3,4} It is important that the experimental dataset is not used for the development of the model. In the end, the experimental and simulation data must match, which can be assessed with root-mean-square errors (RMSEs), with adequate accuracy.³ If not, further circles of parameter refining can be necessary or maybe certain effects on the reaction were overlooked.^{3,4} The finalized model can be a useful tool for process optimization; it can provide knowledge for conducting the process in an economically feasible way or to scale it up.^{1–4} It can also help for designing new processes and identifying possible bottlenecks, such as inhibition by substrates or products and how to handle them, e.g., by finding the optimal feed rate.^{2,3,7} The development of an enzyme kinetic model can also be a tool for identifying the catalytic mechanism of an enzyme.

In this study, we developed a kinetic model for the bienzymatic redox neutral cascade combining a Baeyer–Villiger monoxygenase (BVMO) and an alcohol dehydrogenase (ADH) in a convergent cascade fashion in which cyclohexanone and 1,6-hexanediol are converted to ϵ -caprolactone. Herein, our study is dedicated to find an optimal model that describes the multivariant multienzymatic reaction system with the best fitness quantified by RMSE analysis.

RESULTS AND DISCUSSION

Our recent study on the BVMO-ADH convergent cascade revealed that a newly designed combinatorial mutant of cyclohexanone monoxygenase (CHMO) from *Acinetobacter calcoaceticus*, namely, CHMO M16 DS, is the most efficient variant, with respect to total turnover number.⁸ In all analyses, ADH from *Thermoanaerobacter ethanolicus* (TeSADH)^{9,10} was applied. The kinetic parameters of the CHMO M16 DS were already determined via initial rate measurements,⁸ and it was observed that the CHMO variant, such as wild type (WT), suffers from substrate and product inhibition. Herein, it is worthwhile to mention that the catalytic mechanism of BVMOs is known.¹¹ Because of these observed inhibition issues, only low substrate concentrations were incorporated in the study represented here. Furthermore, crude cell extracts, instead of purified enzymes, were used to simplify the enzyme production. The use of crude cell extract furthermore has the advantage that H₂O₂ that formed as a possible byproduct¹¹ can be degraded by catalase present in the *E. coli* lysate.

Kinetics Modeling of Convergent Cascade: Model 1. In our previous study on the BVMO-ADH cascade high byproduct formation of cyclohexanol (CHL) (Scheme 2), which resulted from the TeSADH-catalyzed reduction of CHO, was observed.⁸ After adjusting the ADH concentration to lower amounts, no significant CHL formation was detected (≤ 0.1 mM). Therefore, this side reaction was not considered in the kinetics model analyzed here. The reaction scheme for the convergent cascade with annotated reaction rates is shown in Scheme 2.

Within the TeSADH reaction, two intermediates are formed: 6-hydroxyhexanal and the respective lactol (oxepan-2-ol), which is a cyclized form of the hemiacetal. For simplicity, the intermediates were considered as one compound: lactol intermediate (LAC). Datasets with progress curves of different substrate and enzyme composition were then generated (see Table SI 1 in the Supporting Information).

The CHMO M16 DS kinetic equation was determined previously with the initial rates analyses.⁸ For TeSADH, competitive substrate and product inhibition was considered. Since CHO is a possible substrate of TeSADH, it was considered as a competitive inhibitor as well. The kinetics equations used in the model can be found in eqs SI(1)–SI(5) in the Supporting Information.

Table 1. Kinetic Parameters in Model 1

v_{\max} [U/mg]	$K_{M,Sub}$ [mM]	$K_{M,Sub}$ [mM]	$K_{i,Sub}$ [mM]	$K_{i,Prod}$ [mM]	$K_{i,pot,Sub}$ [mM]	v_{\max} [U/mg]	$K_{M,Sub}$ [mM]	$K_{M,Sub}$ [mM]
CHMO M16 DS Reaction								
$v_{\max 1}$	$K_{M1,CHO}$	$K_{M1,NADPH}$	$K_{i1,CHO}$	$K_{i1,ECL}$				
8.4	0.002	0.002	30	75				
TeSADH Reaction Step 1								
$v_{\max 2a}$	$K_{M2,1,6-HD}$	$K_{M2,NADP^+}$	$K_{i2,1,6-HD}$	$K_{i2,LAC}$	$K_{i2,CHO}$	$v_{\max 2aR}$	$K_{M2a,LAC}$	$K_{M2a,NADPH}$
4.25	0.1	0.1	100	2	50	0.5	1	0.1
TeSADH Reaction Step 2								
$v_{\max 2b}$	$K_{M2b,LAC}$		$K_{i2b,LAC}$		$K_{i2b,1,6-HD}$			
6	2		2		100			
Evaporation, Autohydrolysis, Deactivation, Degradation Constants [min^{-1}]						Deactivation Constant [$\text{min}^{-1} \text{mM}^{-1}$]		
$K_{d,CHO}$	$k_{d,ECL}$	$k_{d,NADPH}$	$k_{d,NADP^+}$	$k_{dT,M16DS}^a$		$k_{dS,M16DS}^b$	$k_{dS,TeSADH}^b$	
0.0006	0.0002	0.0005	0.0005	0.0003		0.0007	0.0002	

^a k_{dT} Deactivation constant, enzyme deactivation by substrate. ^b k_{dS} Deactivation constant, enzyme deactivation by substrate.

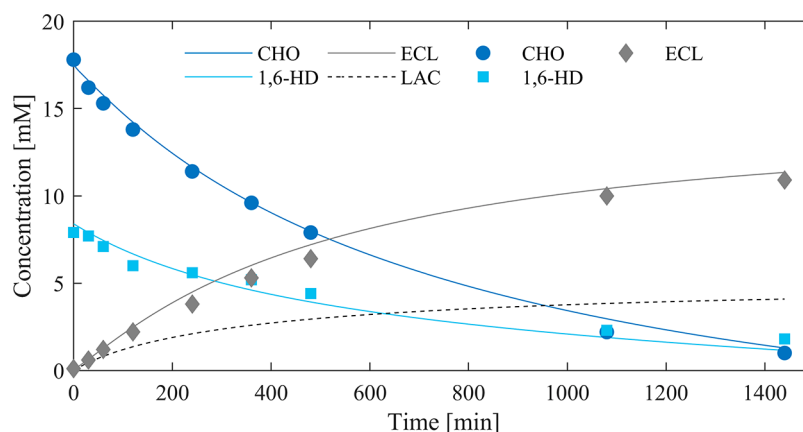


Figure 2. Simulation Model 1 with data overlay. Experimental data are represented by symbols: dark blue circles, CHO; light blue squares, 1,6-HD; gray diamonds, ECL. Lines are simulated progress curves from Model 1 (black lines denote LAC; other colors correspond to the symbols for each compound). Reaction conditions: 100 mM Tris-HCl pH 8, 20 mM CHO, 10 mM 1,6-HD, 0.5 mM NADP⁺, 2 mg/mL (0.033 mM) CHMO M16 DS, 0.005 mg/mL (0.00013 mM) TeSADH. Enzyme preparation as crude cell extract, amounts refer to target enzyme. Dataset A6 was used for this plot.

The initial kinetic parameters were based on literature data^{10,12} or logical assumption. The CHMO M16 DS parameters were taken from the previous study.⁸ The kinetics of TeSADH for 1,6-HD was estimated by Bornadel et al.¹² The evaporation, autohydrolysis, and thermal deactivation constants were determined experimentally (see Table SI 2 in the Supporting Information). The latter, although being analyzed under long-term storage conditions, could be applied in progressive curve analyses. The parameters were then varied within certain boundaries (see Tables SI 3 and SI 4 in the Supporting Information), and the resulting simulations were evaluated visually. To solve the differential equations, MATLAB with an ode45 solver was used. The differential equations were solved solely based on the kinetic parameters given, without considering the experimental data. However, the experimental data was used for the visual evaluation. The resulting kinetic parameters that gave the best fit with dataset A6 (Figure 2) are shown in Table 1.

The simulated progress curves with the overlaid experimental data are shown in the following figures. Figure 2 shows the simulation and data used to develop the model (dataset A6, Table SI 1). This dataset will be referred to as template data for Model 1 in the following. Afterward, the reaction conditions were changed to use half of the CHMO M16 DS concentration (Figure SI 1, dataset A1, in the Supporting Information) and double TeSADH concentration (Figure SI 2, dataset A7, in the

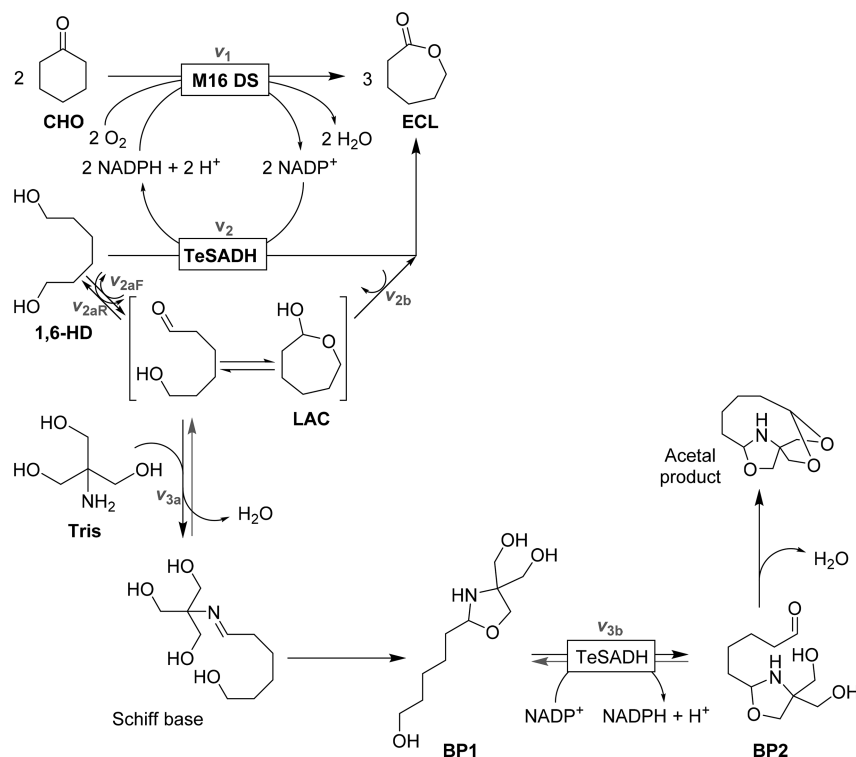
Supporting Information), compared to the template data set (A6). Something that became obvious during the model development process was, that the simulation of the ECL concentration would only fit the experimental data, when not all consumed 1,6-HD is converted to ECL. The change in the concentration of LAC could only be shown as simulated concentrations. With the used analytical method, determination of the LAC intermediate (representing the hemiacetal or cyclic form) was not possible.

In experiment A1 (see Figure SI 1) an abrupt decrease of CHO within 30 min was observed. This behavior could not be elucidated completely, yet. In addition to the visual evaluation, the root mean square error (RMSE) value was calculated (Table 2). Changing the BVMO concentration, compared to the template dataset, resulted in a slight increase of the RMSE from

Table 2. Evaluation of Model 1 under Different Reaction Conditions via Root Mean Square Error (RMSE)

dataset	CHMO [mg/mL]	TeSADH [mg/mL]	RMSE [mM]	RMSE ^a [%]
A6	2.0	0.005	3.79	13
A1	1.0	0.005	4.20	14
A7	2.0	0.01	5.52	18
A4	1.0	0.2	12.03	40

^aPercentage based on a total substrate concentration of 30 mM.

Scheme 3. Reaction Scheme of the Convergent Cascade Including Side Reaction of TeSADH with the Buffer Component Tris^a

^aLegend: CHO, cyclohexanone; 1,6-HD, 1,6-hexanediol; ECL, ϵ -caprolactone; LAC, lactol; BP1, byproduct 1; and BP2, byproduct 2. Reversible reaction that were considered irreversible in the model are shown with gray arrows. Side reaction scheme with Tris buffer adapted from Dithugoe et al.¹³

3.8 mM to 4.2 mM (from 13% to 14%). Nevertheless, the simulation does not fit well to the CHO and ECL concentrations determined experimentally. But the 1,6-HD reaction course is represented very well by the model. When the ADH concentration was doubled, the RMSE increased to 5.5 mM (18%), and the deviation of the simulation from the experimental data was visually detectable for all compounds (see Figure SI 2). When the ADH concentration was increased even more, the RMSE increased from 3.8 mM to 12.0 mM (from 13% to 40%) and it becomes also visually obvious that the model is not accurate under these conditions (see Figure SI 3 in the Supporting Information).

Kinetics Modeling of Convergent Cascade: Model 2.

Since Model 1 could not describe the cascade accurately, the strategy for the model development was changed. For once, other datasets (Table SI 5 in the Supporting Information) were generated and incorporated in the model development. These sets also contained controls where one of the substrates was not added to the reaction and no external addition of cofactor was provided. Furthermore, the BVMO concentration in the reactions was increased to verify whether or not the assumption that the BVMO is a limiting factor in the cascade is correct.

As previously mentioned, for the convergent cascade reactions, the enzymes were provided as crude cell extracts. Therefore, the enzyme preparation already contained NADPH and NADP⁺, to some extent. The experiments without an additional cofactor showed that the cascade indeed performed similar to the cascade with an additional cofactor (Figure SI 4 in the Supporting Information). After 24 h approximately the same product concentration of 10 mM was achieved. However, the product concentration with cofactor addition would have been

higher, if the reaction was stopped sooner. Maximum product concentration of 13 mM (corresponding to 43% theoretical yield) was achieved in 8 h in the reaction with the external cofactor, whereas it was about 10 mM without the external cofactor.

Next, reactions without one of the substrates were conducted, respectively. Surprisingly, in the reactions without 1,6-HD addition, 10 mM of CHO were converted, yielding 4 mM of ECL (Figure SI 5 in the Supporting Information). Also, the 1,6-HD was converted in the reactions without CHO; however, no ECL formation was observed (Figure SI 5). In order to get a better understanding whether the cascade would be productive in a fed-batch approach, additional CHO was provided after 8 h (480 min) of reaction (Figure SI 6 in the Supporting Information). In the end, the product yield increased from 10 mM (43%, batch) to 23 mM (52%, fed-batch) compared to the normal batch reaction.

In the meantime, Dithugoe et al.¹⁰ reported that TeSADH is performing a side reaction with Tris buffer. Since it was observed in Model 1 that apparently not all 1,6-HD was converted to ECL, this side reaction was incorporated into the convergent cascade model. The reaction scheme with the annotated reaction rates, considered in Model 2, is shown in Scheme 3. As observed in Model 1, the two intermediates of the convergent cascade reaction of TeSADH are considered as one compound: LAC. The same is true for the Schiff base and the cyclic byproduct 1 (BP1) generated in the chemical side reaction. Byproduct 2 (BP2) generated by TeSADH from BP1 is considered as the sole product, neglecting the further cyclization to the acetal product. Some of the reaction steps, such as the oxidation step from BP1 to BP2 in the side reaction, are

reversible; however, in the kinetics model, they were considered to be irreversible.

The resulting equations (eqs SI(6)–SI(9) in the Supporting Information) for the rates of the new reactions are listed in the Supporting Information. The differential equations were adjusted accordingly. The reaction rate for v_2 remained the same as described in eq SI(2). The CHMO reaction rate was adjusted to represent the sequentially ordered mechanism with incorporated uncompetitive substrate and noncompetitive product inhibition.

As mentioned previously, for the development of Model 1, the kinetic parameters were varied manually and the changes in the fitness of the simulated versus measured data could be immediately observed and quantified via RMSEs. Because of the 29 parameters involved, handling of this approach is not straightforward for progress simulation. The parameter variation was hence automated and the resulting simulation was evaluated using RMSE values. Furthermore, more than one dataset was used to develop Model 2. It was observed that different enzyme batches led to differences in the performance of the convergent cascade. Therefore, incorporating data from different batches should make the model development more robust against discrepancies resulting only from different enzyme batches. The different iterative steps of the model development strategy are listed in Table 3, giving the dataset used for the modeling and

Table 3. Strategy Followed for the Development of Model 2

	modeling of	particularity of the dataset	dataset
1	TeSADH reaction	experiment contained BVMO, ADH, 1,6-HD and cofactor but no CHO	C1
2	convergent cascade	initial rates values for CHMO, TeSADH boundaries from Step 1	A6
3	convergent cascade	lower CHMO concentration	C4
4	convergent cascade refine for K_i values	higher CHO and 1,6-HD concentrations	A5
5	convergent cascade	transfer to normal conditions	A6
6	convergent cascade refine ADH reaction	increased 1,6-HD concentration	B3
7	convergent cascade refine ADH reaction	increased 1,6-HD concentration	B4
8	convergent cascade	transfer to normal conditions	A6
9	convergent cascade	transfer to dataset with same conditions, boundaries from Step 5 and Step 8	B1

which parameters should especially be refined in the step. After each step, new boundaries for the parameter variation were defined, based on the best parameters from the model evaluation. Depending on the step, 5–20 parameter sets were taken into consideration for finding new boundaries. The differential equations were solved by MATLAB via an ODE solver; within this approach, the ode15s solver was used instead of ode45. As with the additional equations and parameters, the problem became too stiff to be solved by ode45.

In order to combine different kinetic parameter values with each other, vectors for the parameters were created. Each parameter vector was a randomly uniform distribution of values between the defined boundaries. Therefore, the values for the 13–22 parameters were combined randomly with each other. The autohydrolysis constants for ECL and the cofactors, the evaporation constant for CHO, and the thermal deactivation

constant for CHMO M16 DS were not varied during the modeling steps.

After step 8, it was observed that the simulations of CHO and ECL concentrations were underestimated, whereas for 1,6-HD, it was performing well. In step 5, however, ECL and 1,6-HD concentrations were highly overestimated, whereas CHO concentration was slightly overestimated. Consequently, the extremes of both boundaries were combined and another step of modeling was performed. For this step, dataset B1 was used instead of dataset A6, although datasets B1 and A6 have the same reaction conditions. It was discovered that, generally, the performance within dataset A was lower than that observed in datasets B and C; therefore, the decision was made to continue refining the parameters with dataset B.

For all the model steps, the evaporation/autohydrolysis/thermal deactivation constants were the experimentally determined ones. In the end, the evaporation constant for CHO was increased slightly, because, in the preliminary experiments, the k_d parameter was slightly underestimating the actual autohydrolysis in the preliminary experiment. For the same reason, the k_d parameter for ECL autohydrolysis was slightly adjusted. The final parameters of the model are listed in Table 4.

The simulated progress curves with the experimental data overlay are shown in Figure 3 and Figures SI 7–SI 9. In none of these datasets, LAC accumulated according to the simulation and, thus, it is not shown in the progress curve plots. Instead, BP2 accumulated in the cascade reactions according to our simulations, whereby, with the analytical method used, no byproduct formation could be detected.

As seen in Model 1, a change in the amount of BVMO caused smaller deviations in the fitness of simulated versus experimental data, compared to a change in ADH amount. In Model 2, there exists no template dataset, since several datasets were used to refine the parameters. For the datasets with 0.005 mg/mL TeSADH, the RMSE was 3–4 mM (10%–13%), whereas, for the higher ADH concentration, the RMSE increased to 6 mM and 21% (see Table 5).

In the preliminary experiments, it was shown that full conversion of 20 mM within 30 min could be achieved with equimolar amounts of NADPH (Figure SI 10 in the Supporting Information). This means that CHMO M16 DS is able to perform the reaction to its full completion, despite CHO inhibition under these conditions. Another indication from these experiments is that there is no or no severe NADPH inhibition using the cofactor at stoichiometric amounts. Thus, with a maximum of 0.5 mM available cofactor during the cascade reaction, cofactor inhibition was negligible. Furthermore, the preliminary experiments showed that the autohydrolysis of ECL could not be neglected. The same was true for evaporation of CHO and degradation of NADPH/NADP⁺. It has been shown in several cases that consideration of the deactivation of the enzyme can provide a better fit of the model.^{14–16} However, not only thermal deactivation should be considered, which can be approximated by the long-term storage stability. The inactivation by reaction components could also have an influence.¹⁴ Combined thermal and CHO-mediated deactivation was hence considered for CHMO M16 DS. However, for TeSADH, only CHO-mediated deactivation was applied. Since TeSADH is a thermostable enzyme (temperature optimum of 90 °C¹⁷), thermal deactivation did not seem very likely at a reaction temperature of 30 °C.

Table 4. Kinetics Parameters in Model 2

v_{\max} [U/mg]	$K_{M,\text{Sub}}$ [mM]	$K_{M,\text{Sub}}$ [mM]	$K_{i,\text{Sub}}$ [mM]	$K_{i,\text{prod}}$ [mM]	$K_{i,\text{pot,Sub}}$ [mM]	v_{\max} [U/mg]	$K_{M,\text{Sub}}$ [mM]	$K_{M,\text{Sub}}$ [mM]
CHMO M16 DS Reaction								
$v_{\max 1}$	$K_{M1,\text{CHO}}$	$K_{M1,\text{NADPH}}$	$K_{i1,\text{CHO}}$	$K_{i1,\text{ECL}}$				
8.39	0.0002	0.002	25.76	35.50				
TeSADH Reaction Step 1								
$v_{\max 2a}$	$K_{M2,1,6\text{-HD}}$	K_{M2,NADP^+}	$K_{i2,1,6\text{-HD}}$	$K_{i2,\text{LAC}}$	$K_{i2,\text{CHO}}$	$v_{\max 2aR}$	$K_{M2a,\text{LAC}}$	$K_{M2a,\text{NADPH}}$
7.72	0.54	0.015	90.07	16.73	44.92	1.19	3.10	0.26
TeSADH Reaction Step 2								
$v_{\max 2b}$	$K_{M2b,\text{LAC}}$		$K_{i2b,\text{LAC}}$		$K_{i2b,1,6\text{-HD}}$			
4.43	2.90		21.96		67.06			
Chemical Reaction and TeSADH Byproduct Formation								
k_{TRIS} [L mmol ⁻¹ min ⁻¹]						$v_{\max 3b}$	$K_{M3,\text{BP1}}$	K_{M3,NADP^+}
6.72						8.31	3.92	0.23
Evaporation, Autohydrolysis, Deactivation, Degradation Constants [min⁻¹]								
$k_{d,\text{CHO}}$	$k_{d,\text{ECL}}$	$k_{d,\text{NADPH}}$	k_{d,NADP^+}	$k_{d,\text{TeSADH}}^a$	$k_{d,\text{TeSADH}}^b$	$k_{d,\text{M16DS}}^b$	$k_{d,\text{TeSADH}}^b$	
0.0002	0.0003	0.0005	0.0003	0.0001	0.0006	0.0003		

^a $k_{d,T}$ Deactivation constant, enzyme deactivation by substrate. ^b $k_{d,S}$ Deactivation constant, enzyme deactivation by substrate.

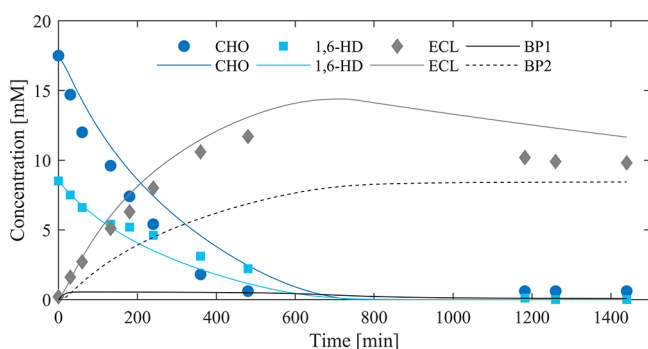


Figure 3. Simulation Model 2 with data overlay. Experimental data is denoted as symbols: dark blue circles, CHO; light blue squares, 1,6-HD; and gray diamonds, ECL. Lines represent simulated progress curves from model 2. Black lines represent BP1 and BP2 (dotted); other colors correspond to the symbols for each compound. Reaction conditions: 100 mM Tris-HCl (pH 8), 20 mM CHO, 10 mM 1,6-HD, 0.5 mM NADP⁺, 2 mg/mL (0.033 mM) CHMO M16 DS, 0.005 mg/mL (0.00013 mM) TeSADH. Enzyme preparation as crude cell extract; amounts refer to the target enzyme. Dataset B1 was used in this plot.

Table 5. Evaluation of Model 2 at Different Reaction Conditions via RMSE

dataset	CHMO [mg/mL]	TeSADH [mg/mL]	RMSE [mM]	RMSE ^a [%]
B1	2.0	0.005	2.99	10
C4	1.5	0.005	4.04	13
C5	3.1	0.005	3.68	12
B2	1.0	0.2	6.30	21

^aPercentage based on a total substrate concentration of 30 mM.

As mentioned previously, the byproduct CHL was obtained from the side reaction of TeSADH with CHO (Scheme 2). Nevertheless, this reaction and the resulting CHL could not be detected after reduction of the ADH amount in the cascade reactions. For TeSADH, competitive inhibition was considered, whereby all considered compounds were possible substrates of TeSADH. Usually, substrate inhibition is considered as uncompetitive, i.e., the inhibitor binds only to the enzyme–substrate complex. However, since all the compounds are in direct concurrence, it was more likely that competitive inhibition is applicable, i.e., the inhibitor binds to the free enzyme. That

substrate inhibition can certainly be competitive for ADHs, which has indeed been described in the literature.^{18,19}

Comparison of Models 1 and 2. In both models, the determined TeSADH kinetic parameters differ from those in the literature.⁸ Compared to the documented kinetics data, in the models developed here, the v_{\max} for the cascade reaction was 40–80 times higher, based on v_{2a} (see Schemes 2 and 3). In addition, the K_M value for 1,6-HD was 4–20 times lower. The main difference was that the kinetic data from the literature was determined via photometric measurements of initial rates. This is challenging for the TeSADH reaction, since it is a two-step oxidation reaction, i.e., enzymatic dehydrogenation/oxidation of a hydroxy group to an aldehyde (v_{2a}) and enzymatic dehydrogenation/oxidation of a hydroxy group to a cyclic ester/lactone (v_{2b}). These two steps cannot be distinguished in a photometric assay. Furthermore, in the initial rate measurements, only the TeSADH reaction was present. The first step of the reaction is reversible; therefore, the determined parameters could be influenced by the reverse/back reaction. Whereas in the process curve analyses, also the BVMO reaction was present, shifting the reaction to the target product side.

Already in the early stages of the model development for the convergent cascade, it became obvious that not all consumed substrates (CHO, 1,6-HD) were converted to the target product ECL.

In Model 1, it was assumed that 1,6-HD was only converted to the hemiacetal, inhibiting the second reaction. This seemed to be a well-fitting model, at least for one dataset. However, the transfer of this assumption to the other reaction conditions showed that the model was not describing the cascade correctly. It became especially eminent when the ADH concentration was increased in the simulations. The model predicted substrate conversion and product formation rates that were higher than those observed in the experiments. Therefore, we suspected that the ADH catalysis was a limiting step of the cascade under these circumstances. However, this could not be observed in the experiments. Nor was the CHMO M16 DS observed to be a limiting factor. When the concentration of the BVMO was increased from 2 mg/mL to 3 mg/mL, only a slight increase in ECL formation was detected (see Figure SI 11 in the Supporting Information). No difference in the CHO reaction course was observed, but a slight change in the 1,6-HD reaction course was detected. This could have been caused by the slightly higher

starting concentration of 1,6-HD in datasets C5 and C6, leading to the higher ECL production. An increase of ADH with 1 mg/mL BVMO also resulted in a slight change in the reaction course (see Figure SI 12 in the Supporting Information). But also, this can be attributed to the slightly higher 1,6-HD concentration in the respective experiment. In the preliminary experiments, it was already determined that the CHMO M16 DS should be able to convert 20 mM CHO within 30 min. Nonetheless, in the cascade reaction, full conversion was achieved earliest within 8 h (480 min). Reasons for that could be that the ADH-mediated cofactor regeneration was not efficient enough and/or other components of the cascade were inhibiting the BVMO.

In Model 1, the deviation between simulation and experimental data was lowest when only the BVMO concentration was changed. This is a hint that it was mainly the ADH reaction that was not captured entirely by the model. When the model was transferred to dataset A1, which had half the BVMO concentration as the template dataset, the RMSE decreased only slightly. In the development of Model 2, the strategy was changed. Not only was one dataset used to model the reaction: several were used. As already implemented for Model 1, the model was developed without direct modeling against the experimental data. This was inspired by the technique developed by Finnigan et al.⁷ Since the cascade was very complex with a vast amount of unknown parameters, the datasets were used to refine the model by finding boundaries (see Tables SI 3 and SI 4) with the best fit to the experimental data. In addition, another approach was considered: modeling first only the individual reactions to find starting parameters for the model.⁴ Afterward, different datasets were used to refine the model parameters. Furthermore, the BVMO reaction equation was switched from normal Michaelis–Menten with uncompetitive substrate and noncompetitive product inhibition to an equation that describes the sequentially ordered mechanism of the reaction. A sequentially ordered mechanism should give a better description of the BVMO kinetics and has been used in models previously, using 2-propanol as a cosubstrate for cofactor regeneration.²⁰ During the initial rate measurements for CHMO M16 DS, it was determined that the inhibition is already eminent at a concentration of 20 mM CHO. Thus, it is not negligible in the model developed here. At the end, the inhibition terms were introduced in the respective parts of the equation that are associated with the inhibitor complexes.²¹

During the iterative steps of model refinement, a dataset with 50 mM CHO was applied. However, it was observed that, with the higher CHO concentration, the model was not giving a good fit. This had been also observed when applying the final Model 1 and Model 2 to higher CHO concentrations. This was most likely due to the aforementioned oxygen limitation in the case of higher CHO concentrations. Since oxygen as a third substrate of the BVMO reaction was not incorporated in the model, it is not applicable to higher CHO concentrations. Consequently, the inhibition terms could perhaps not be captured entirely, since high concentrations were not modeled successfully. For BVMO, these were determined with initial rate measurements; however, the final model had a lower K_i value for ECL than that determined with the initial rates.

Other control experiments with an additional supply of CHO, after 8 h of reaction time, showed that the BVMO is still active after that time (see Figure SI 6 in the Supporting Information). However, the reaction rate was lower, most likely because of deactivation of the CHMO. During the characterization of the CHMO M16 DS, a half-life time of 116 h at 30 °C was

determined,⁷ which was only under storage conditions. It was already expected that, during the process, the stability would be lower. Most of the deactivation may occur due to H₂O₂ formation in the catalytic cycle of the BVMO via a short cut.^{11,22–24} In other control experiments, it was observed that the reaction of the BVMO with CHO produced only small amounts of H₂O₂. However, exact determination was not possible, because the Ampliflu Red assay²⁵ reacted with CHO and, hence, only high amounts of hydrogen peroxide would have been detectable. Nonetheless, the CHO-supply control experiment (Figure SI 6) also showed that, with a continuous substrate feed, higher yields of ECL could be obtained. Here, note that, because of higher ECL yield, the inhibition of CHMO M16 DS, as well as the autohydrolysis of the target product ECL, must be handled carefully. This can be done either by removal of the product through absorption^{26,27} or by in situ ring-opening polymerization (ROP).²⁸ The latter has not been efficiently implemented in an enzymatic cascade for ECL synthesis. So far, only oligo-ECL instead of polycaprolactone (PCL) was formed directly in the cascade.²⁸ Because of the equilibrium reaction, there is also a risk that the oligo-ECL could hydrolyze again.^{29,30}

Here, it must be emphasized that the TeSADH reaction is unfortunately still a “black box”. To eliminate the unnecessary side reactions, both enzymes should be purified for a general model development. Between datasets A and B/C, a high difference in the performance of the cascade was observed, which could have resulted from (i) the activities of the enzymes, especially from the BVMO was different between enzyme batches; and (ii) the quantification of the enzyme amounts was based on SDS-PAGE analysis, which was not accurate enough. Alternatively, instead of using concentrations, units of the enzymes for their activities can be implemented in the cascade. After knowing that the side chemical reaction due to the Tris buffer is not negligible, an alternative buffer system (e.g., phosphate buffer) could be used. Phosphate buffer was not chosen initially because the stability of the nicotinamide cofactors is negatively influenced by it.³¹ In addition, glycine NaOH buffer gave lower CHMO stabilities, compared to the Tris buffer (data not shown) seen in our preliminary studies.

Overall, our study showed that Model 2 seemed to have a better description of the cascade reaction than Model 1. The RMSE for the simulation of dataset B1 was 10% better than that observed for Model 1 (dataset A6, 13%; see Tables 2 and 5). Increasing the ADH concentration, compared to these conditions, caused, in both cases, a higher RMSE value. However, in Model 2, the RMSE with 21% was 2-fold lower than that observed for Model 1 (40%; see Tables 2 (dataset B2) and 5 (dataset A4)). For refinement of the ADH kinetic parameters, more datasets would be necessary.

CONCLUSIONS

In the work presented herein, CHMO M16 DS was implemented in the convergent cascade coupled with TeSADH for the synthesis of ECL. Preliminary experiments showed that the BVMO was able to convert 20 mM CHO within 30 min, when equimolar NADPH was supplied. Hence, 20 mM CHO was chosen as the substrate concentration for further experiments. Moreover, it was verified that, at 30 °C, significant autohydrolysis of ECL occurred, which must be considered and addressed in the future development of the cascade. Possible solutions could be absorption of ECL on a resin or in-situ polymerization to PCL.^{24–26} The latter has been shown in organic media to a great extent, yet polymerization in aqueous

media has still its faults.^{26,27,30} On the other hand, in an alternative case, the ECL was hydrolyzed intentionally, to lower the inhibition of the CHMO in the cascade.³² The generated 6-hydroxyhexanoate can still be polymerized to PCL via a lipase in organic media.³²

The preliminary optimization study⁸ had shown that a reduction in the amount of TeSADH was possible and necessary to reduce the side reaction resulting in CHL. As a consequence, the byproduct formation of CHL was reduced to ≤ 0.1 mM and was not considered further in the development of the kinetic models for the convergent cascade.

Model 1 of the cascade considered only the convergent cascade reaction without side reactions. It was noticed that the cosubstrate 1,6-HD was not fully converted to ECL, but it was anticipated that inhibition of the second step of the TeSADH reaction was the cause.

Recently, Opperman and co-workers described that the intermediate of the TeSADH reaction, 6-hydroxyhexanal, was undergoing a chemical reaction with the Tris buffer.¹³ A subsequently formed byproduct BP1 was then further converted by TeSADH to another byproduct BP2.¹³ Therefore, in Model 2, this side reaction was implemented. The conversion of BP1 to BP2 by TeSADH also provided the cofactor regeneration that the second step in the TeSADH reaction would have provided. Generally, the use of purified enzymes would lead to precise control of the cascade system, but one must remember that it would be too expensive, especially for a bulk chemical.³³ Using whole cells would reduce the costs of enzyme production and could potentially increase the stability of the BVMO. Nonetheless, as already shown by Kohl et al.,³⁴ balancing the ratio of the BVMO and the ADH in the cells is very important. Since this has already been managed for the linear cascade, resulting in a more efficient cascade,^{34,35} we have no doubt that this will also be possible for the convergent cascade.

EXPERIMENTAL SECTION

Materials and Methods. All chemicals were purchased from VWR International (Denmark) and Carl Roth and used as received.

Quantification of Enzymes. The estimation of CHMO M16 DS and TeSADH was as described in the work of Engel et al.,⁸ but the gels were scanned and analyzed in a Gel Doc™ EZ Imager (BioRad). The software used was Image Lab (BioRad), instead of ImageJ.

Cascade Reactions. The convergent cascade reaction were performed in 100 mM Tris-HCl (pH 8), in a volume of 1 mL in 35-mL glass vessels. 0–100 mM CHO, 0–50 mM 1,6-HD, 0.5 mM NADP⁺, 1–3.1 mg/mL (0.016–0.05 mM) CHMO M16 DS and 0.005–0.2 mg/mL (0.00013–0.005 mM) TeSADH were used in the reactions. The enzymes were supplied as crude cell extracts, and the concentrations refer to the amount of the respective target enzyme in the extract. The mixtures were incubated in a shaking incubator with 120 rpm and 30 °C for up to 24 h.

GC-Analytics. From the cascade reactions, 25 μ L samples were taken in different time intervals and extracted with 250 μ L of ethyl acetate containing 5 mM dodecane as an internal standard. After centrifugation, 200 μ L of the ethyl acetate phase was transferred to a new tube and dried with MgSO₄. The sample was centrifuged to separate the drying agent and the organic phase and was analyzed afterward via gas chromatography (GC). For analysis, a Nexis GC-2030 system coupled with a flame ionization detector (Shimadzu) and equipped with a β -

DEX™ 120 capillary column (30 m \times 0.25 mm, d_f 0.25 μ m, Supelco Sigma-Aldrich) was used. The temperature profile is shown in Table SI 6 in the Supporting Information.

Simulations. The kinetic models were developed with the aid of MATLAB scripts (The MathWorks, Inc., Natick, MA). Differential equations were solved via ode45 (Model 1) or ode15s (Model 2). In the development of Model 2, the boundaries for each iterative step were found within the parameter combinations, with the best RMSE being 5–10. Depending on the step, 100–100 000 simulations were performed with different parameter values and combinations.

ASSOCIATED CONTENT

Supporting Information

The Supporting Information is available free of charge at <https://pubs.acs.org/doi/10.1021/acs.oprd.0c00372>.

All control experiments, tables for the datasets, and the corresponding reaction conditions, as well as equations used in the simulations (PDF)

AUTHOR INFORMATION

Corresponding Author

Selin Kara – Department of Engineering, Biocatalysis and Bioprocessing Group, Aarhus University, 8000 Aarhus, Denmark; orcid.org/0000-0001-6754-2814; Email: selin.kara@eng.au.dk

Authors

Jennifer Engel – Department of Engineering, Biocatalysis and Bioprocessing Group, Aarhus University, 8000 Aarhus, Denmark

Uwe T. Bornscheuer – Department of Biotechnology and Enzyme Catalysis, Institute of Biochemistry, Greifswald University, 17489 Greifswald, Germany; orcid.org/0000-0003-0685-2696

Complete contact information is available at: <https://pubs.acs.org/10.1021/acs.oprd.0c00372>

Notes

The authors declare no competing financial interest.

ACKNOWLEDGMENTS

Authors J.E. and S.K. acknowledge the financial support from German Research Foundation (Deutsche Forschungsgemeinschaft, Grant No. KA 4399/1-1). The authors thank Assoc. Prof. Dr. Diederik J. Opperman (University of the Free State, South Africa) for the plasmid harboring CHMO M16 DS, as well as Kim Møller Johansen and Michelle Leganger Juul Sørensen for their technical support. Furthermore, author J.E. would like to thank Jannis Reich, for his kind help with MATLAB, and Frederic Perz, for fruitful discussions.

ABBREVIATIONS

CHMO, cyclohexanone monooxygenase; ADH, alcohol dehydrogenase; CHO, cyclohexanone; 1, 6-HD, 1,6-hexanediol; BP, byproduct; LAC, lactol intermediate; ECL, ϵ -caprolactone; PCL, polycaprolactone; v , reaction rate [mM/min]; ODE, ordinary differential equations; v_{\max} , maximum reaction rate [U/mg]; K_M , Michaelis–Menten constant [mM]; K_i , inhibition constant [mM]; dc/dt , rate of component concentration change [mM/min]; c_{compound} , compound concentration [mM]; c_{enzyme} , enzyme concentration, based on density [mg/mL]; c'_{enzyme}

enzyme concentration, based on molality [mM]; $k_{\text{hydrolysis, evap, degra}}$ hydrolysis, evaporation, degradation rate constant [min^{-1}]; k_{ds} enzyme deactivation rate constant [$\text{mM}^{-1} \text{min}^{-1}$]

REFERENCES

- (1) Straathof, A. J. J. Development of a Computer Program for Analysis of Enzyme Kinetics by Progress Curve Fitting. *J. Mol. Catal. B: Enzym.* **2001**, *11*, 991–998.
- (2) Zavrel, M.; Kochanowski, K.; Spiess, A. C. Comparison of Different Approaches and Computer Programs for Progress Curve Analysis of Enzyme Kinetics. *Eng. Life Sci.* **2010**, *10*, 191–200.
- (3) Vasic-Racki, D.; Findrik, Z.; Vrsalovic Presecki, A. Modelling as a Tool of Enzyme Reaction Engineering for Enzyme Reactor Development. *Appl. Microbiol. Biotechnol.* **2011**, *91*, 845–856.
- (4) Al-Haque, N.; Santacoloma, P. A.; Neto, W.; Tufvesson, P.; Gani, R.; Woodley, J. M. A Robust Methodology for Kinetic Model Parameter Estimation for Biocatalytic Reactions. *Biotechnol. Prog.* **2012**, *28*, 1186–96.
- (5) Muschiol, J.; Peters, C.; Oberleitner, N.; Mihovilovic, M. D.; Bornscheuer, U. T.; Rudroff, F. Cascade Catalysis-Strategies and Challenges En Route to Preparative Synthetic Biology. *Chem. Commun. (Cambridge, U. K.)* **2015**, *51*, 5798–811.
- (6) Palmer, T.; Bonner, P. L., 8 - Enzyme Inhibition. In *Enzymes*, Second Edition; Palmer, T., Bonner, P. L., Eds.; Woodhead Publishing, 2011; pp 126–152.
- (7) Finnigan, W.; Cutlan, R.; Snajdrova, R.; Adams, J. P.; Littlechild, J. A.; Harmer, N. J. Engineering a Seven Enzyme Biotransformation Using Mathematical Modelling and Characterized Enzyme Parts. *ChemCatChem* **2019**, *11*, 3474–3489.
- (8) Engel, J.; Mthethwa, K. S.; Opperman, D. J.; Kara, S. Characterization of New Baeyer-Villiger Monooxygenases for Lactonizations in Redox-Neutral Cascades. *Mol. Catal.* **2019**, *468*, 44–51.
- (9) Li, C.; Heatwole, J.; Soelaiman, S.; Shoham, M. Crystal Structure of a Thermophilic Alcohol Dehydrogenase Substrate Complex Suggests Determinants of Substrate Specificity and Thermostability. *Proteins: Struct., Funct., Genet.* **1999**, *37*, 619–627.
- (10) Bryant, F. O.; Wiegel, J.; Ljungdahl, L. G. Purification and Properties of Primary and Secondary Alcohol Dehydrogenases from *Thermoanaerobacter Ethanolicus*. *Appl. Environ. Microbiol.* **1988**, *54*, 460–465.
- (11) Fürst, M. J. L. J.; Gran-Scheuch, A.; Aalbers, F. S.; Fraaije, M. W. Baeyer-Villiger Monooxygenases: Tunable Oxidative Biocatalysts. *ACS Catal.* **2019**, *9*, 11207–11241.
- (12) Bornadel, A.; Hatti-Kaul, R.; Hollmann, F.; Kara, S. A Bi-Enzymatic Convergent Cascade for E-Caprolactone Synthesis Employing 1,6-Hexanediol as a 'Double-Smart Cosubstrate'. *ChemCatChem* **2015**, *7*, 2442–2445.
- (13) Dithugoe, C. D.; van Marwijk, J.; Smit, M. S.; Opperman, D. J. An Alcohol Dehydrogenase from the Short-Chain Dehydrogenase/Reductase Family of Enzymes for the Lactonization of Hexane-1,6-Diol. *ChemBioChem* **2019**, *20*, 96–102.
- (14) Ohs, R.; Leipnitz, M.; Schopping, M.; Spiess, A. C. Simultaneous Identification of Reaction and Inactivation Kinetics of an Enzyme-Catalyzed Carboligation. *Biotechnol. Prog.* **2018**, *34*, 1081–1092.
- (15) Abmann, M.; Stöbener, A.; Mügge, C.; Gaßmeyer, S. K.; Hilterhaus, L.; Kourist, R.; Liese, A.; Kara, S. Reaction Engineering of Biocatalytic (S)-Naproxen Synthesis Integrating in-Line Process Monitoring by Raman Spectroscopy. *React. Chem. Eng.* **2017**, *2*, 531–540.
- (16) Pesci, L.; Baydar, M.; Glueck, S.; Faber, K.; Liese, A.; Kara, S. Development and Scaling-up of the Fragrance Compound 4-Ethylguaiacol Synthesis Via a Two-Step Chemo-Enzymatic Reaction Sequence. *Org. Process Res. Dev.* **2017**, *21*, 85–93.
- (17) Ziegelmann-Fjeld, K. I.; Musa, M. M.; Phillips, R. S.; Zeikus, J. G.; Vieille, C. A *Thermoanaerobacter Ethanolicus* Secondary Alcohol Dehydrogenase Mutant Derivative Highly Active and Stereoselective on Phenylacetone and Benzylacetone. *Protein Eng., Des. Sel.* **2007**, *20*, 47–55.
- (18) Taber, R. L. The Competitive Inhibition of Yeast Alcohol Dehydrogenase by 2,2,2-Trifluoroethanol. *Biochem. Educ.* **1998**, *26*, 239–242.
- (19) Oestreicher, E. G.; Pereira, D. A.; Pinto, G. F. Steady-State Kinetic Mechanism of *Thermoanaerobium Brockii* Alcohol Dehydrogenase: A Study of Discrimination between Alternative Kinetic Models. *J. Biotechnol.* **1996**, *46*, 23–31.
- (20) Hogan, M. C.; Woodley, J. M. Modelling of Two Enzyme Reactions in a Linked Cofactor Recycle System for Chiral Lactone Synthesis. *Chem. Eng. Sci.* **2000**, *55*, 2001–2008.
- (21) Morrison, J. F. Enzyme Activity: Reversible Inhibition. In *eLS*, **2001**, DOI: 10.1038/npg.els.0000600.
- (22) Mihovilovic, M. D. Baeyer-Villiger Oxidations. In *Enzyme Catalysis in Organic Chemistry*; Drauz, K., Gröger, H., Eds.; Wiley-VCH Verlag GmbH & Co. KGaA: Weinheim, Germany, 2012; pp 1439–1485.
- (23) de Gonzalo, G.; Mihovilovic, M. D.; Fraaije, M. W. Recent Developments in the Application of Baeyer-Villiger Monooxygenases as Biocatalysts. *ChemBioChem* **2010**, *11*, 2208–31.
- (24) Ryerson, C. C.; Ballou, D. P.; Walsh, C. Mechanistic Studies on Cyclohexanone Oxygenase. *Biochemistry* **1982**, *21*, 2644–2655.
- (25) Morlock, L. K.; Böttcher, D.; Bornscheuer, U. T. Simultaneous Detection of NADPH Consumption and H₂O₂ Production Using the Ampliflu (Tm) Red Assay for Screening of P450 Activities and Uncoupling. *Appl. Microbiol. Biotechnol.* **2018**, *102*, 985–994.
- (26) Hilker, I.; Gutierrez, M. C.; Furstoss, R.; Ward, J.; Wohlgemuth, R.; Alphand, V. Preparative Scale Baeyer-Villiger Biooxidation at High Concentration Using Recombinant *Escherichia Coli* and *in Situ* Substrate Feeding and Product Removal Process. *Nat. Protoc.* **2008**, *3*, 546–54.
- (27) Hilker, I.; Alphand, V.; Wohlgemuth, R.; Furstoss, R. Microbial Transformations, 56. Preparative Scale Asymmetric Baeyer-Villiger Oxidation Using a Highly Productive "Two-in-One" Resin-Based *in Situ* Sfrp Concept. *Adv. Synth. Catal.* **2004**, *346*, 203–214.
- (28) Schmidt, S.; Scherkus, C.; Muschiol, J.; Menyes, U.; Winkler, T.; Hummel, W.; Groger, H.; Liese, A.; Herz, H. G.; Bornscheuer, U. T. An Enzyme Cascade Synthesis of Epsilon-Caprolactone and Its Oligomers. *Angew. Chem., Int. Ed.* **2015**, *54*, 2784–7.
- (29) Reisky, L.; Srinivasamurthy, V. S. T.; Badenhorst, C. P. S.; Godehard, S. P.; Bornscheuer, U. T. A Novel High-Throughput Assay Enables the Direct Identification of Acyltransferases. *Catalysts* **2019**, *9*, 64.
- (30) Engel, J.; Cordellier, A.; Huang, L.; Kara, S. Enzymatic Ring-Opening Polymerization of Lactones: Traditional Approaches and Alternative Strategies. *ChemCatChem* **2019**, *11*, 4983.
- (31) Anderson, B. M.; Anderson, C. D. The Effect of Buffers on Nicotinamide Adenine Dinucleotide Hydrolysis. *J. Biol. Chem.* **1963**, *238*, 1475–1478.
- (32) Scherkus, C.; Schmidt, S.; Bornscheuer, U. T.; Gröger, H.; Kara, S.; Liese, A. A Fed-Batch Synthetic Strategy for a Three-Step Enzymatic Synthesis of Poly- α -Caprolactone. *ChemCatChem* **2016**, *8*, 3446–3452.
- (33) Tufvesson, P.; Lima-Ramos, J.; Nordblad, M.; Woodley, J. M. Guidelines and Cost Analysis for Catalyst Production in Biocatalytic Processes. *Org. Process Res. Dev.* **2011**, *15*, 266–274.
- (34) Kohl, A.; Srinivasamurthy, V.; Böttcher, D.; Kabisch, J.; Bornscheuer, U. T. Co-Expression of an Alcohol Dehydrogenase and a Cyclohexanone Monooxygenase for Cascade Reactions Facilitates the Regeneration of the NADPH Cofactor. *Enzyme Microb. Technol.* **2018**, *108*, 53–58.
- (35) Srinivasamurthy, V. S. T.; Böttcher, D.; Engel, J.; Kara, S.; Bornscheuer, U. T. A Whole-Cell Process for the Production of E-Caprolactone in Aqueous Media. *Process Biochem.* **2020**, *88*, 22–30.